Electronic Supporting Information

Anion vacancy correlated photocatalytic CO_2 to CO conversion over quantum-confined CdS nanorods under visible light

Qing Guo,[a,c] Shu-Guang Xia,[a,c] Zhi-Kun Xin,[a,c] Yang Wang,[a,c] Fei Liang,[b,c] Xiao-Lei Nan,[a,c] Zhe-Shuai Lin,[b,c] Xu-Bing Li,*[a,c] Chen-Ho Tung[a,c] and Li-Zhu Wu*[a,c]

*a*Key Laboratory of Photochemical Conversion and Optoelectronic Materials, Technical Institute of Physics and Chemistry, Chinese Academy of Sciences, Beijing 100190, People's Republic of China
*b*Key Laboratory of Functional Crystals and Laser Technology, Technical Institute of Physics and Chemistry, Chinese Academy of Sciences, Beijing 100190, People's Republic of China.
*c*School of Future Technology, University of Chinese Academy of Sciences, Beijing 100049, People's Republic of China.

*To whom correspondence should be addressed.

E-mail: lixubing@mail.ipc.ac.cn; lzwu@mail.ipc.ac.cn;

Telephone: (+86) 10-8254-3580; *Fax:* (+86) 10-8254-3580.

Table of Contents

1. Synthesis of CdS nanorods: In order to accurately control the size and shape of CdS, a traditional hot injection method was involved with employing CdO and S power as precursors. In a typical synthetic procedure, 15 mg CdO, 1.5 g trioctylphosphine oxide (TOPO), 77 mg octadecylphosphonic acid (ODPA), 25 mg hexylphosphonic acid (HPA) were added into a 25 mL flask. The mixture was heated to above 300 ºC until solution colourless under Ar flow. The temperature of mixture was heated to 370 ºC, 0.4 mL TOP dissolved 32 mg sulphur power as S stock solution was injected. Because reaction time could affect ripening and growth of nanocrystals. During the experiments, the reaction vessel was maintained at 370 ºC for 5 seconds after the injection of S precursors to control the first absorption peak of nanocrystals at ~440 nm, and then quickly cooling down to quench the growth of nanocrystals. In order to ensure the similar size distribution while different surface properties, we control the process of cooling down after reaction. As the volatilization of solvent could take away heat quickly, during the process, acetone and ethanol were chosen to spray reaction bottle to bring away heat. The spray speed was controlled. We found the fast spraying results in more S vacancy, while slow spraying leads to less S vacancy. After the solution was cooled down to room temperature quickly, the product was collected and washed with n-hexane and precipitated with methyl alcohol several times to remove excess organic compounds.[1] The obtained organic-ligand capped CdS samples were dispersed in n-hexane for optical characterization or further use.

Ligand exchange: Organic ligand on surface of CdS nanorods exchanged was performed in water solution.[2] Briefly, 15 mL water containing 100 µL 3-mercaptopropionic acid (3-MPA), was tuned to pH = 10 by the addition of NaOH aqueous solution to form an aqueous solution. Then, 5 mL of organic-ligand capped CdS n-hexane solution was added, and the mixture was vigorously stirred overnight at R.T. The obtained product was washed with acetone to remove organic ligands. Then, the 3-MPA capped CdS were dispersed in a small amount of water and precipitated again by adding an excess amount of ethanol. This process was repeated several times to remove the unbonded 3-MPA. Finally, CdS was dispersed in water for photocatalytic experiments.

2. Synthesis of $Cd_{0.95}Ag_{0.1}S$ nanorods: Ag substituting of the CdS nanorods was realized through a standard cation-exchange procedure.[3, 4] In this procedure, CdS nanorods were dispersed in 6 mL n-hexane firstly, and the mole number of Cd atom was calculated according formula [Cd] in ppb =

82043.2*OD-694.9 (OD is absorbance value of CdS). $AgNO_3$ was dissolved in 1.0 mL methyl alcohol, and the content of Ag was 1.0% [Cd]. $AgNO_3$ solution was added to CdS n-hexane solution drop wise. After added, the solution was vigorously stirred for 1.0 h. Excess methyl alcohol was added to precipitate and then solid was washed several times.

3. Photocatalytic experiments: Firstly, CdS water solution was precipitated by the addition of isopropanol and dispersed in dimethyl formamide (DMF). Then 1.0 mL triethylamine (TEA) was added to 5 mL CdS DMF solution (c = 1.0×10^{-6} mol/L) and the solution was degassed by bubbling CO_2 for 30 min. Then 600 μL ultrapure CH_4 was injected into the system to work as the internal standard for quantitative GC analysis. The generated gas in the reaction headspace was analyzed by using a gas chromatograph (*Shimadzu* GC2014CAFC/APC) equipped with a thermal conductivity detector and 5 Å molecular sieve GC columns. Ar was used as the carrier gas. The response factors for H_2/CH_4 and CO/CH_4 were about 4.45 and 0.39 under the experimental condition, respectively, which was established by calibration with known amounts of H_2, CO and CH_4, and determined before and after measurements. Error bars on H_2 and CO were calculated from at least three independent experiments.

4. Electrochemical measurements: Electrochemical Impedance Spectroscopy curves were recorded by Zennium electrochemical workstation (Germany, Zahner Company) with a three-electrode electrochemical cell in 0.1 M Na_2SO_4 electrolyte under visible-light irradiation (λ = 450 nm). The resultant electrode served as the working electrode, platinum as the counter electrode and Ag/AgCl (3.0 M KCl) electrode as the reference electrode. The working electrodes were prepared by adding 20 μL Nafion (5%) aqueous solution into a 1.0 mL CdS n-hexane solution. The obtained slurry was then spread onto FTO glass substrate with an active area of about 1.0 cm^2. The film was dried under inert atmosphere before electrochemical measurements.

5. DFT calculations: the DFT calculations were performed by the CASTEP package[5] with the ultrasoft pseudopotentials and GGA-PW91 functional.[6] A 400 eV plane wave basis cutoff energy was used throughout our calculations. The convergence thresholds between optimization cycles for energy change and maximum force were set as 5.0×10^{-6} eV/atom and 0.03 eV/Å, respectively. The Monkhorst-Pack grids[7] of 2 ×2×1 *k*-points were used for the (001) surface of wurtzite CdS. In this work, we constructed stoichiometric slabs of 12.40 Å × 12.40 Å ×10.89 Å (eight atomic layers) with a vacuum

thickness of 15 Å to model the (001) surface of CdS. In all calculations, the atoms in the bottom layers were fixed, but the atoms in the two topmost layers, as well as C, O and H atoms, were allowed to relax. The geometry structure of the isolated CO_2 molecule was optimized using a supercell of 15 Å × 15 Å × 15 Å. The calculated C-O bond length and bond angle (O-C-O) were 1.171 Å and 180.0°, which were in good agreement with the experimental values.

Taking CO_2 as an example, the adsorption energy was defined as,[8]

$$E_{ads} = E_{(CO_2 + slab)} - [E_{(CO_2)} + E_{(slab)}]$$

where the first term is the total energy of the slab with the adsorbed CO_2 molecule on the surface, the second term is the total energy of isolated CO_2 molecule, and the third term is the total energy of the bare slab of the surface (perfect or S-vacancy slab). According to the above definitions, a negative E_{ads} value corresponds to an exothermic adsorption, and the more negative the E_{ads}, the stronger the adsorption.

6. Enlarged STEM image of CdS nanorods
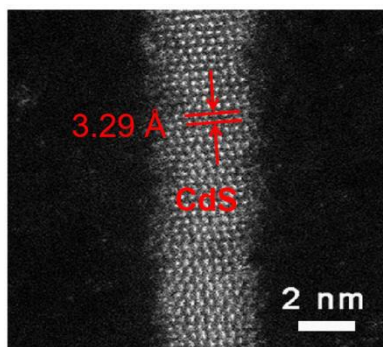
Fig. S1 High-resolution aberration-corrected scanning transmission electron microscopy (STEM) image of the obtained CdS nanorods.

7. Full XPS spectrum of CdS nanorods
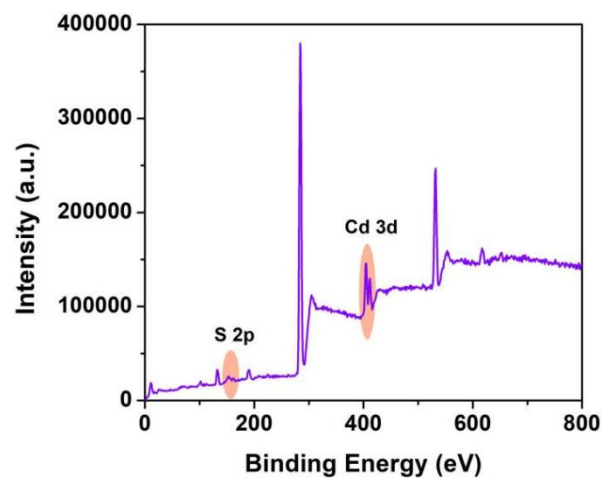
Fig. S2 Full XPS spectrum of the obtained CdS nanorods, indicating that both of Cd and S were found in the sample.

8. EPR spectrum of CdS nanorods
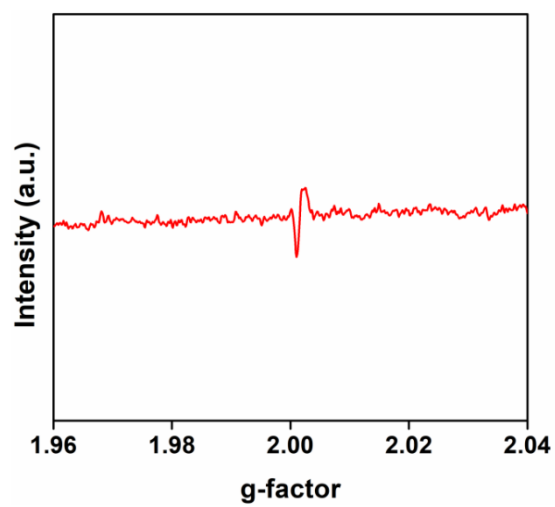
Fig. S3 Electron paramagnetic resonance (EPR) spectrum of CdS nanorods in n-hexane solution at room temperature.

9. XPS analysis of surface compositions of CdS nanorods
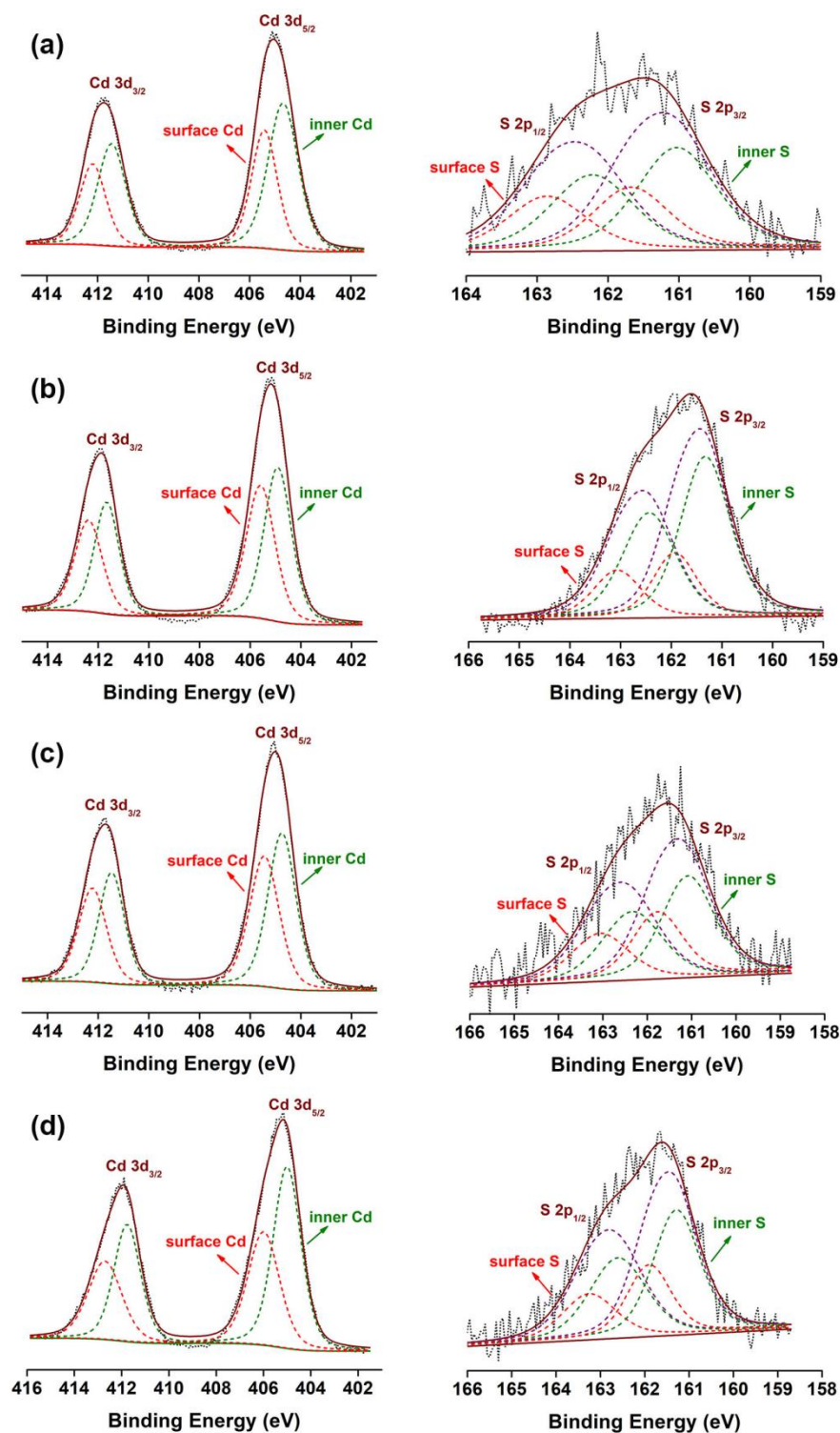
Fig. S4 XPS raw data and Gaussian fitting peaks of Cd and S signals in CdS nanorods for (a) CS-1, (b) CS-2, (c) CS-3 and (d) CS-4. Green fitted peaks indicate signals from inner Cd (S) atoms while red dot lines represent signals from surface atoms of CdS nanorods.

10. Table S1. Summary of integrated areas of fitting peaks of Cd and S elements from XPS analysis

Sample	Areas of Cd element				Surface Cd (%)	Areas of S element				Surface S (%)	Whole Cd/S atom ratio
	Cd 3d$_{5/2}$		Cd 3d$_{3/2}$			S 2p$_{1/2}$		S 2p$_{3/2}$			
	inner	surface	inner	surface		inner	surface	inner	surface		
CS-1	24962.96	17016.57	16143.57	11830.48	41.24	455.62	299.49	578.20	332.64	37.94	2.977/1
CS-2	35582.39	32222.86	23170.41	21132.69	47.6	1826.87	631.85	1285.14	509.77	26.8	1.916/1
CS-3	16340.38	14432.54	10609.46	9812.749	47.36	338.23	224.47	435.35	271.54	39.07	3.05/1
CS-4	38077.22	26948.77	23482.09	19760.87	43.14	757.84	395.45	972.3	515.4	34.61	3.11/1

11. PL lifetime of CdS nanorods
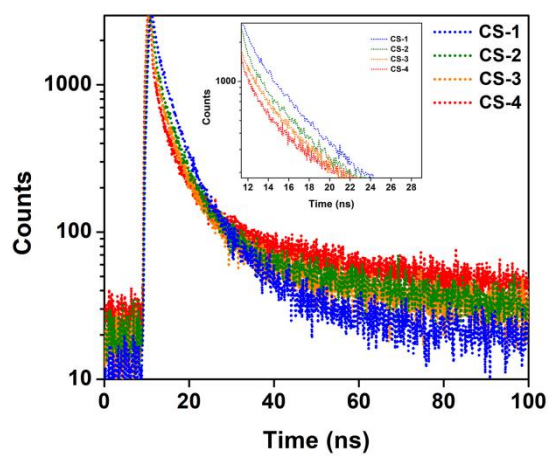
Fig. S5 Time-resolved PL spectra of CdS with different concentrations of S vacancy.

12. Table S2. Fitted parameter of PL lifetime in Fig. S5

Samples	B1	B2	τ_1 / ns	τ_2 / ns	τ / ns
CS-1	2077.758	1128.58	1.9736	6.5746	4.9
CS-2	0.118	0.03	0.9881	5.4247	3.6
CS-3	0.083	0.016	0.5173	4.7331	3.2
CS-4	0.114	0.012	0.4438	4.5915	2.6

Photogenerated carriers lifetime of CdS nanorods with different concentrations of surface S vacancy were fitted with double-exponential function Y(t) based on nonlinear least-squares, using the following equation:

$$Y(t) = B_1 \exp(-t / \tau_1) + B_2 \exp(-t / \tau_2)$$

Where B_1, B_2 are fractional contributions from time-resolved emission decay lifetime τ_1, τ_2, as shown in **Table S2**. The average lifetime τ could be obtained from the following equation:

$$<\tau> = \frac{B_1\tau_1^2 + B_2\tau_2^2}{B_1\tau_1 + B_2\tau_2}$$

As displayed in **Fig. S5**, with the increase of S vacancy, the lifetime of CdS was decayed from CS-1 to CS-4 with 4.9 ns to 2.6 ns (**Table S2**).

13. Isotopic experiment using $^{13}CO_2$ as reactant
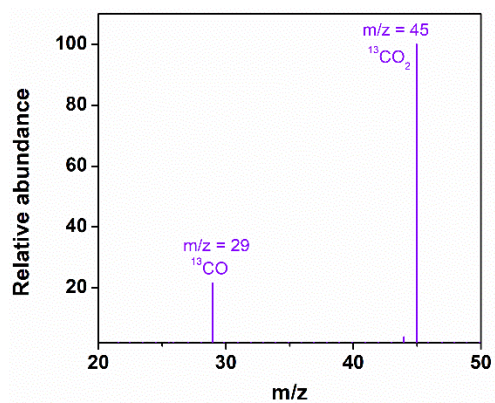
Fig. S6 GC–MS analysis of reduction product using $^{13}CO_2$ as the reactant.

14. VB XPS spectra of CdS nanorods
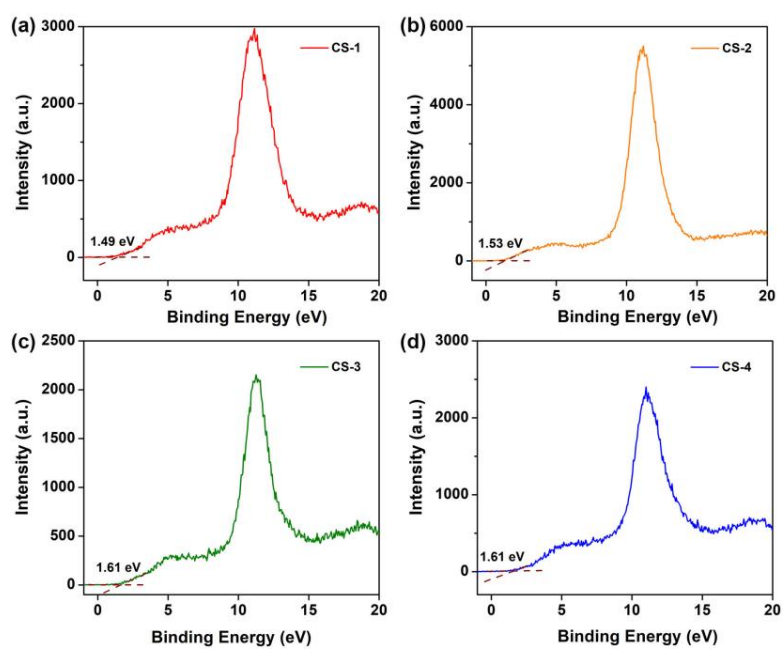
Fig. S7 High-resolution valence band XPS spectra of CdS nanorods. As shown in Fig. S7, the valence bands of CdS are +1.49 V, +1.53 V, +1.61 V and +1.61 V vs. NHE for CS-1, CS-2, CS-3 and CS-4, respectively.

15. Calculated band-gaps of CdS nanorods
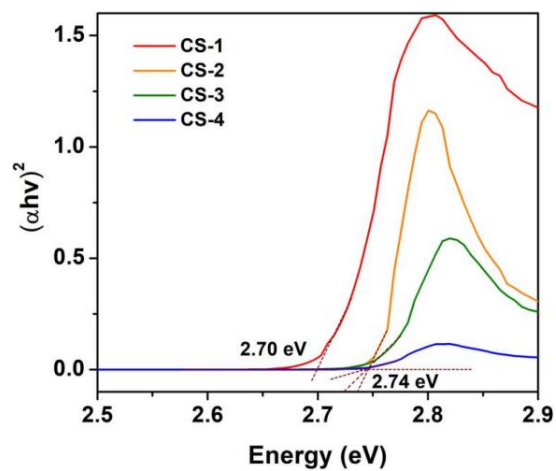
Fig. S8 The corresponding *Tauc plots* of CdS nanorods in n-hexane from UV-vis absorption spectra. We found that

CdS could give the approximate band gaps from ~2.70 eV to ~2.74 eV.

16. TEM image of CdS after Ag$^+$ ions exchange
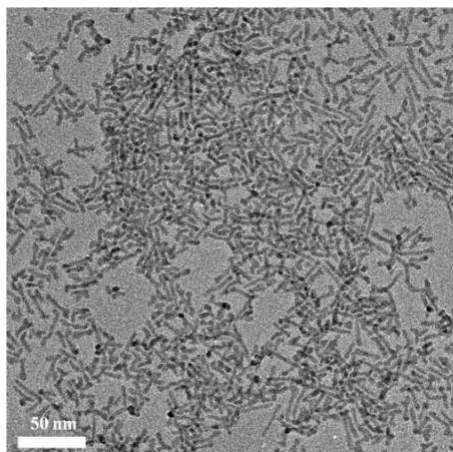
Fig. S9 TEM image of CdS nanorods after exchanging with Ag$^+$ ions. As shown in Fig. S9, the rod-shape of CdS remains unchanged after Ag$^+$ ions exchange.

17. UV-vis absorption spectra of CdS after Ag⁺ ions exchange
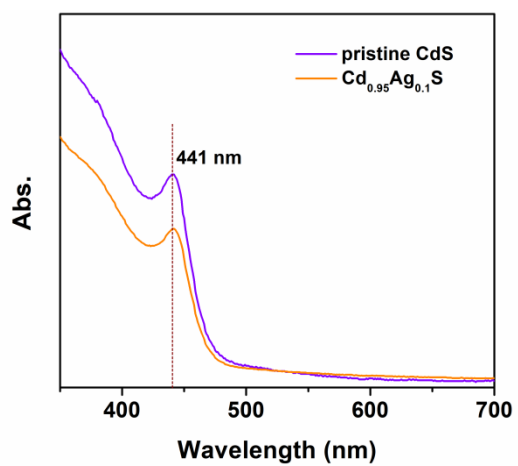
Fig. S10 UV-vis absorption spectra of CdS nanorods before and after Ag⁺ ions exchange via a cation-exchange process.

18. Steady-state PL spectrum of CdS after Ag⁺ ions exchange
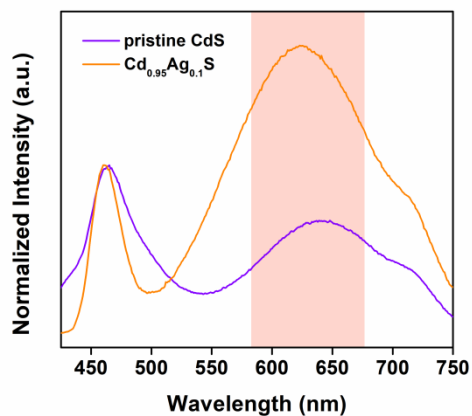
Fig. S11 Normalized PL spectra (with excitation of 400 nm laser) of pristine CdS and CdS after Ag⁺ ions exchange in n-hexane at room temperature.

19. Table S3. The calculated adsorption energy of CO_2 and CO on CdS after Ag^+ ions exchange

Sample	Adsorption energy of CO_2 (eV)	Adsorption energy of CO (eV)
CdS	-0.078	-0.049
$Cd_{0.95}Ag_{0.1}S$	-0.041	-0.348

20. The interaction between CO_2 molecules and $Cd_{0.95}Ag_{0.1}S$
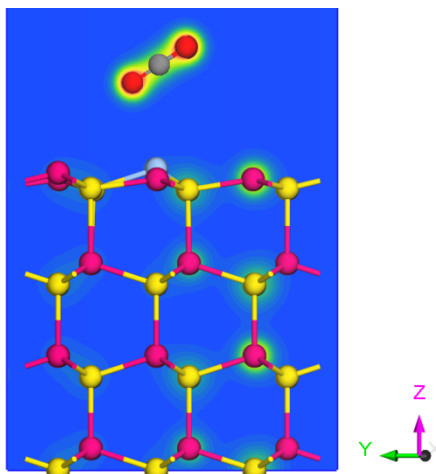
Fig. S12 The scheme of adsorption of CO_2 molecule on the surface of $Cd_{0.95}Ag_{0.1}S$. The pink, yellow, blue, red and gray balls represent Cd, S, Ag, C and O atoms, respectively. As shown in Fig. S12, the adsorption CO_2 was not on Ag or Cd site on surface.

21. Electrochemical impedance spectra of CdS nanorods
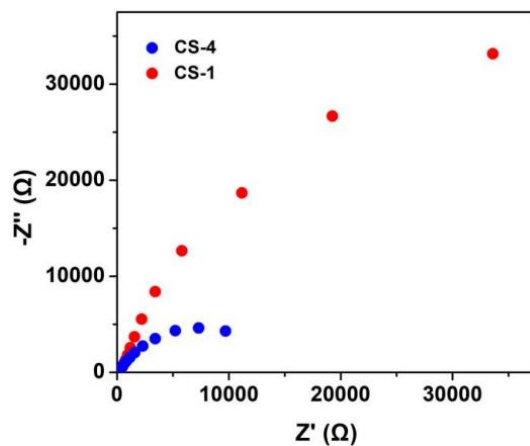
Fig. S13 Electrochemical impedance spectra of CdS nanorods for CS-1 and CS-4 in 0.1 M Na_2SO_4 aqueous solution

with a standard three-electrode system under visible-light irradiation (λ = 450 nm).

22. Reference

1. L. Carbone, C.Nobile, D. M. Giorgi, D. F. Sala, G. Morello, P. Pompa, M. Hytch, E. Snoeck, A. Fiore, R. I. Franchini, M. Nadasan, F. A. Silvestre, L.Chiodo, S. Kudera, R. Cingolani, R. Krahne and L. Manna, *Nano Lett*., **2007**, *7*, 2942-2950.

2. P. Wang, J. Zhang, H. He, X. Xu and Y. Jin, *Nanoscale* **2015,** *7*, 5767-5775.

3. J. L. Fenton and R. E. Schaak, *Angew Chem Int Ed* **2017**, *56*, 6464-6467.

4. O. Elimelech, J. Liu, A. M. Plonka, A. I. Frenkel and U. Banin, *Angew Chem Int Ed* **2017,** *56*, 10335-10340.

5. S. J. Clark, M. D. Segall, C. J. Pickard, P. J. Hasnip, M. J. Probert, K. Refson and M. C. Payne, *Zeitschrift Fur Kristallographie* **2005,** *220*, 567-570.

6. J. P. Perdew, K. Burke and M. Ernzerhof, *Phys. Rev. Lett.* **1996,** *77*, 3865-3868.

7. H. J. Monkhorst and J. D. Pack, *Phys. Rev. B* **1976,** *13*, 5188-5192.

8. J. Ran, G. Gao, F. T. Li, T. Y. Ma, A. Du and S. Z. Qiao, *Nat Commun* **2017,** *8*, 13907.